Isomeric $\frac{13}{2}^+$ $(\nu i_{\frac{13}{2}}^{-1})$ state in ^{211}Th

K. Auranen,[1,*] J. Uusitalo,[1] H. Badran,[1,†] T. Grahn,[1] P. T. Greenlees,[1] A. Herzáň,[1,2] U. Jakobsson,[1] R. Julin,[1] S. Juutinen,[1] J. Konki,[1] M. Leino,[1] A.-P. Leppänen,[3] G. O'Neill,[1,4,‡] J. Pakarinen,[1] P. Papadakis,[1,§] J. Partanen,[1,‖] P. Peura,[1] P. Rahkila,[1] P. Ruotsalainen,[1] M. Sandzelius,[1] J. Sarén,[1] C. Scholey,[1,¶] L. Sinclair,[1,5] J. Sorri,[1,†] S. Stolze,[1,#] and A. Voss[1]

[1]*University of Jyvaskyla, Department of Physics, P.O. Box 35, FI-40014 University of Jyvaskyla, Finland*

[2]*Institute of Physics, Slovak Academy of Sciences, SK-84511 Bratislava, Slovakia*

[3]*Radiation and Nuclear Safety Authority - STUK, Lähteentie 2, 96400 Rovaniemi, Finland*

[4]*University of Liverpool, Department of Physics, Oliver Lodge Laboratory, Liverpool L69 7ZE, United Kingdom*

[5]*Department of Physics, University of York, Heslington, York YO10 5DD, United Kingdom*

(Received 2 September 2020; accepted 13 May 2021; published 25 May 2021)

Using a fusion-evaporation reaction and a gas-filled recoil separator, an isomeric state [$T_{\frac{1}{2}} = 83(8)$ μs] with a most likely spin and parity of $\frac{13}{2}^+$ has been identified in ^{211}Th. The isomeric state is mainly depopulated via a hindered internal $M2$ transition [$B(M2) = 0.0025(5)$ W.u.], but also a weak α-decay branch of 4(3)% was observed. The present observations fit well to the systematic pattern set by the previously identified states of the same spin and parity in this region of the nuclear chart.

DOI: 10.1103/PhysRevC.103.054323

I. INTRODUCTION

Isomeric excited states [1] have a particularly important role in fundamental nuclear physics, as well as in its applications. Metastable states provide opportunities from energy storage to medicine [2,3] and might play a role in stellar processes [4]. From the perspective of experimental nuclear physics, the isomeric states offer unique opportunities for experimental arrangements in the form of isomeric targets (see, for example, Ref. [5]) and isomeric beams [6,7]. More commonly, however, the metastable states are used to gain information on nuclear structure; if one measures the energy, rate, and multipole of the transition depopulating the level, an access is gained to the underlying transition matrix element. Furthermore, the decay of the isomeric state might populate otherwise inaccessible intermediate state(s) that in turn can be studied, for example, on a focal plane of a recoil separator [8,9], or said transitions can be used to gain high selectivity in the form of a recoil-isomer decay tagging [10–12].

In this article we report the discovery of an isomeric state in ^{211}Th with, most likely, spin and parity of $^{13}/_2^+$ arising from the $\nu i_{13/2}^{-1}$ configuration. States of the same I^π and configuration are fairly well established through polonium, radon, and radium isotopes with even Z, odd N, and $N < 126$; see, for example, Refs. [13–17] and references therein. Among the $N < 126$ isotopes of thorium, only two examples of the $^{13}/_2^+$ state were proposed before this study in ^{209}Th [18] and ^{213}Th [19]. The dominant depopulation mechanism of the isomer appears to be internal transition in isotopes close to the $N = 126$ shell closure, whereas α decay takes over when one moves on the nuclear chart towards the proton dripline. Some of the observed internal decay paths involve a rare transition of $M4$ type [14,20]. When it comes to ^{211}Th, we have observed a dominant internal cascade as well as a weak α-decay branch from the metastable state.

II. EXPERIMENTAL DETAILS

The nuclei of interest were generated in a fusion-evaporation reaction ^{181}Ta(^{36}Ar, $1p5n$)^{211}Th. The results reported here represent the sum of the data obtained under the experimental conditions listed in Table I. The K-130 cyclotron of the University of Jyväskylä was used to deliver the ion beams, and the fusion-evaporation residues recoiling out from the target, referred to as recoils hereinafter, were selected from the primary beam using the recoil ion transport unit (RITU) [21,22] gas-filled recoil separator. The recoils passed through a multiwire proportional counter (MWPC) at the focal plane of RITU before implantation into a double-sided silicon strip detector (DSSD) of the GREAT spectrometer [23]. The individual strips of the DSSD were gain matched using a ^{133}Ba source (low-energy range for internal-conversion events) or

*kalle.e.k.auranen@jyu.fi

†Present address: Radiation and Nuclear Safety Authority - STUK, Laippatie 4, 00880 Helsinki, Finland.

‡Present address: Department of Physics, University of York, Heslington, York YO10 5DD, United Kingdom.

§Present address: STFC Daresbury Laboratory, Daresbury, Warrington WA4 4AD, United Kingdom.

‖Deceased.

¶Present address: MTC Limited, Ansty Park, Coventry CV79JU, United Kingdom.

#Present address: Physics Division, Argonne National Laboratory, 9700 South Cass Avenue, Lemont, Illinois 60439, USA.

TABLE I. The reactions, beam energies $E_b^{\rm lab}$ and intensities I_b, irradiation times t, and the thicknesses of the tantalum target d_{Ta} and of the downstream carbon degrader foil d_C used at different phases of this study.

Phase	Reaction	$E_{\rm b}^{\rm lab}$ (MeV)	$I_{\rm b}$ (pnA)	t (h)	$d_{\rm Ta}$ ($\frac{\mu g}{cm^2}$)	$d_{\rm C}$ ($\frac{\mu g}{cm^2}$)
1	^{36}Ar + ^{181}Ta	178	141	8.2	1000	70
2	^{36}Ar + ^{181}Ta	184	138	14.4	450	70
3	^{36}Ar + ^{181}Ta	190	190	15.3	1000	70
4	^{36}Ar + ^{181}Ta	196	196	20.9	1000	70
5	^{36}Ar + ^{181}Ta	202	199	42.3	1000	70
6	^{36}Ar + ^{181}Ta	208	210	68.8	1000	70
7	^{36}Ar + ^{181}Ta	214	158	16.2	1000	70
8	^{36}Ar + ^{181}Ta	210	180	80.6	1000	70

α-decay data collected through a ^{36}Ar + ^{169}Tm reaction during the back-to-back sister experiment of this study, whose results are already published [24]. An energy resolution of approximately 25 keV (FWHM, α-decay events) was obtained for the DSSD. The highly pixelated (1 mm^2 pixel size) 300-μm-thick DSSD was used to correlate spatially the recoil-implantation events to the subsequent decay events. Recoils were distinguished from the scattered primary beam and other unwanted beam- and target-like ions based on their energy loss in the MWPC and the MWPC-DSSD time of flight, and an event without the MWPC signal was considered as a decay event. As demonstrated in Fig. 1, many of the α-particle energies are overlapping in this region of the nuclear chart. It is therefore necessary to seek correlations up to four consecutive decay events in order to achieve reliable identification of the parent nucleus. The α-decay tagging efficiency was further enhanced by assembling 28 silicon PIN diodes in a tunnel geometry upstream from the DSSD to detect α particles escaping from the implantation detector. Similar to

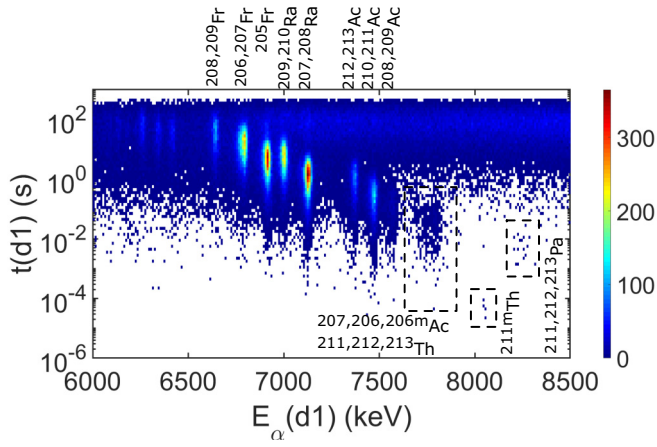

FIG. 1. Measured decay time, as a function of the α-particle energy, of the first decay event of a decay chain consisting of two to four decay events correlated with a recoil implantation event in the same pixel of the DSSD. Some of the previously known [27,28] activities are labeled as well as the newly observed α decay of the isomeric state in ^{211}Th.

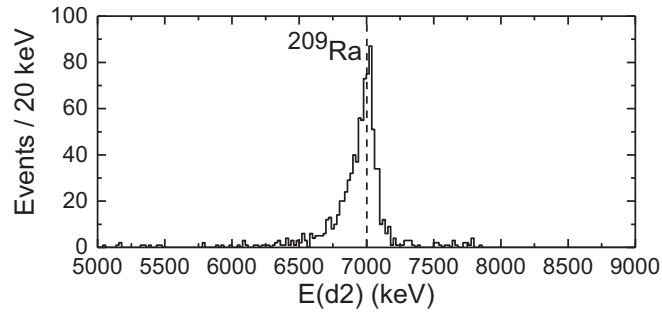

FIG. 2. α-particle energy spectrum reconstructed from the α particles that escaped from the DSSD, but which were detected in any of the PIN diodes surrounding the DSSD. ^{209}Ra events were selected by setting decay-time conditions of $t(d1) < 1$ ms and $t(d2) < 16$ s, i.e., by gating with the internal-conversion electrons of a transition depopulating a known isomeric state in ^{209}Ra [16] [see Sec. III for the definition of $E(dn)$ and $t(dn)$]. The dashed line is the α-particle energy of ^{209}Ra reported in the literature [27].

the DSSD, the PIN diodes were calibrated by using the α-decay data obtained via the reaction of Ref. [24]. A correction was applied to account for the varying effective thickness of the dead layers on the surface of the DSSD and the PIN diodes as a function of the α-particle emission angle. An example α-particle energy spectrum obtained from the escape events by adding back the energy measured in the PIN diodes is displayed in Fig. 2, and it reflects an energy resolution of approximately 120 keV (FWHM). Furthermore, γ rays at the focal plane were measured by using three clover-type germanium detectors [25] around the GREAT vacuum chamber and one planar-type detector inside, immediately behind the DSSD. Data from all detector channels were recorded independently and time stamped with a 100 MHz clock. The data were presorted into correlated decay chains containing two to four decay events using the GRAIN [26] software package. The final analysis of the decay chains was carried out in the MATLAB R2018b environment.

III. OBSERVATIONS

The observations described in this section were obtained by selecting those event chains where a recoil implantation event was followed by two to four consecutive decay events in the same pixel of the DSSD. $E(dn)$ and $t(dn)$ denote the measured particle energy and decay time of the nth decay event in the chain, respectively. The proposed decay scheme of the isomeric $13/2^+$ ($\nu i_{13/2}^{-1}$) state in ^{211}Th is displayed in Fig. 3, and the experimental evidence supporting this decay pattern is provided below and discussed further in Sec. IV.

A. Internal decay of the isomer

The energy correlation plot of the first and second decay event following a recoil implantation is displayed in Fig. 4(a). Here time gates of $t(d1) < 0.5$ ms and $t(d2) < 160$ ms were set, of which the former is to select fast decay events likely originating from isomeric states, and the latter is approximately 4–5 times the half-life of ^{211}Th and ^{212}Th. The two

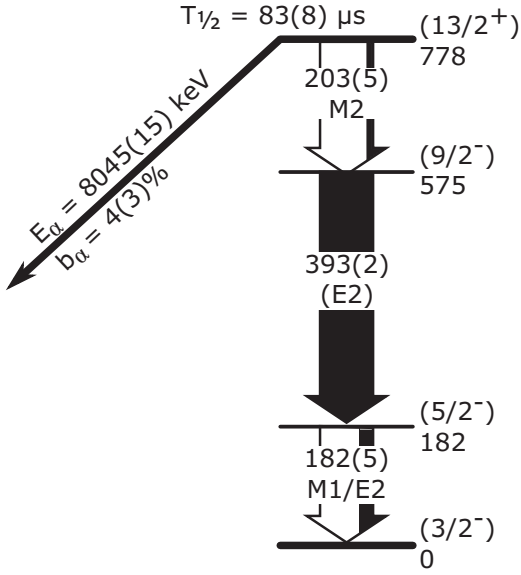

FIG. 3. Decay scheme of the $^{13}/_2^+$ $(\nu i_{13/2}^{-1})$ isomeric state in ^{211}Th observed in this study

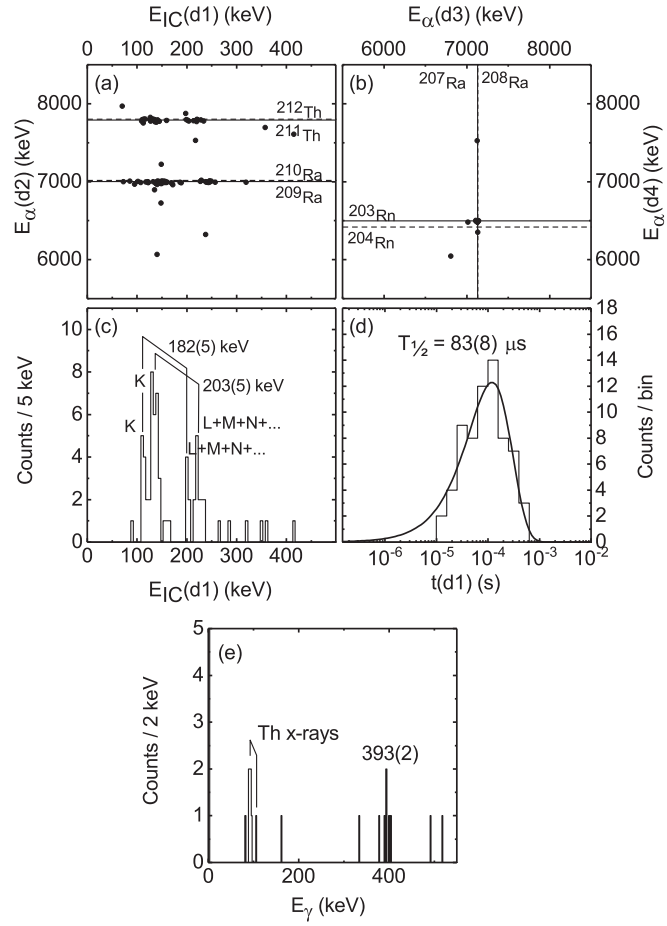

FIG. 4. (a) Correlated decay events observed in the DSSD within the decay-time conditions of $t(d1) < 0.5$ ms and $t(d2) < 160$ ms. (b) The decay events following those of panel (a) in the same pixel of the DSSD. The solid and dashed lines in panels (a) and (b) are selected α-particle energies obtained from the literature [29–35]. (c) Energy spectrum of internal-conversion electrons emitted in the decay of the newly observed isomeric state in ^{211}Th and (d) the respective decay-time distribution with a least-squares fit (solid line [36]) to the data. (e) Energy spectrum of γ rays in coincidence with the electrons of panel (c). See text for further details.

event groups represent the internal-conversion electrons arising from the depopulation of a known isomeric state in ^{209}Ra [16], and a newly observed one either in ^{211}Th or in ^{212}Th. As demonstrated in Fig. 1, many of the α-particle energies in the region are overlapping. Therefore it is necessary to search decays down to the fourth decay generation in order to pinpoint the mother isotope of thorium with the metastable state. These correlations are displayed in Fig. 4(b). As the $E(d4)$ corresponds to the α-particle energy of ^{203}Rn, the newly observed isomeric state must be in ^{211}Th.

The energy spectrum of the internal-conversion electrons associated with the depopulation of the ^{211m}Th is displayed in Fig. 4(c). This spectrum was obtained by demanding the aforementioned time conditions, and in addition that either $E(d2)$ *or* $E(d3)$ must reflect the literature α-particle energy of ^{211}Th or ^{207}Ra, respectively. The tagging efficiency was further enhanced by adding back the α-particle energy of those decays where the α particle escaping the DSSD was caught by the PIN diodes. Detection efficiencies of 55% and 25% for the DSSD and the PIN diodes, respectively, reflects a probability of 96% to observe at least one of the two α particles with full energy either in the implantation detector, or in the surrounding PIN tunnel. The four peaks in the spectrum fit the K and $L + M + \cdots$ energies of the 182(5) and 203(5) keV transitions. The sum peaks of the two transitions are expected to be present in a level of a few counts, some of the events on the high-energy side of Fig. 4(c) may exhibit this origin. It is noteworthy that the response of the implantation detector involves the energy of the emitted internal-conversion electron summed with the energy released in the subsequent atomic relaxation via low-energy x rays or Auger electrons as the atomic vacancies created by the internal-conversion decays are filled [37,38]. These atomic phenomena were accounted for as the transition energies were deduced. Furthermore, fast decay events will pile up with the preceding signal from the recoil implantation, which will interfere with the energy extraction. An internal correction curve was created, and, finally, the corrected spectrum is displayed in Fig. 4(c). See the Appendix for details.

For the 203-keV transition a $\frac{K}{L+M+\cdots}$ intensity ratio of 2.1(4) was extracted that fits the value of 2.1(3) obtained with the BrIcc calculator [39] for a 203-keV $M2$ transition. Hence we assign $M2$ character for this transition. Similarly, the experimental intensity ratio of 1.7(6) reflects the theoretical value of 2.0(3) for a 182-keV $M2$ transition; however, the total number of 182-keV conversion events in Fig. 4(c) is smaller than that observed for the 203-keV transition, in contrast with theoretical total internal-conversion coefficients. Furthermore, the measured intensity ratio is between the theoretical values of 4.0(4) and 0.248(13) obtained for pure $M1$ and $E2$ type 182-keV transitions, respectively. Therefore we propose a mixed $M1/E2$ character for the 182-keV transition.

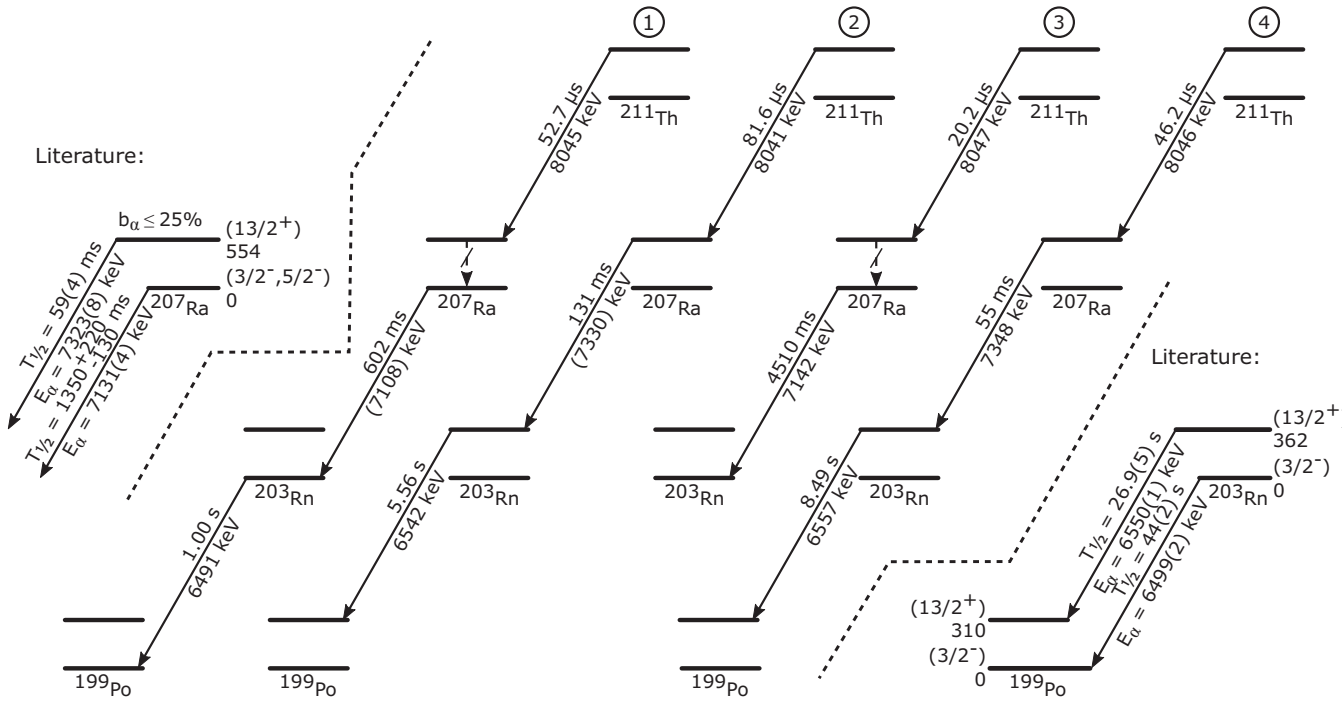

FIG. 5. Decay correlations and the respective recorded decay data of the four α-decay chains originating from the metastable state of ^{211}Th observed in this study. The α-particle energies reconstructed from an escape event observed in the PIN diodes are indicated with parentheses. The internal cascade (marked with $\overset{\downarrow}{\gamma}$) from the $(13/2^+)$ state to the ground state of ^{207}Ra was not observed. For comparison, the relevant literature data [33,40,41] are provided above (below) the dashed line.

The decay-time distributions of both transitions are similar, suggesting a cascade, and the sum distribution is displayed in Fig. 4(d). A half-life of 83(8) μs was obtained via a least-squares fitting method described in Ref. [36]. Furthermore, a 393(2) keV γ ray [see Fig. 4(e)] was observed to coincide with the electrons of Fig. 4(c) once the γ-ray data from the focal-plane clover array are summed with that from the planar detector.

B. α decay of the isomer

Altogether, four α-decay events from the newly observed isomeric state of ^{211}Th were observed during this study, which are highlighted in Fig. 1. The recorded decay data and correlations are displayed in Fig. 5 together with the relevant literature values. We interpret the number two and four chains to be links between the isomeric $(13/2^+)$ states of ^{199}Po, ^{203}Rn, ^{207}Ra, and the newly observed isomeric state of ^{211}Th. Chain number one (three) connects the ground state α decays of ^{203}Rn and ^{207}Ra to the α decay of ^{211m}Th via an internal cascade, which was not observed in this study. An upper limit of $b_\alpha \leqslant 25\%$ was deduced for the α-decay branch of ^{207m}Ra in Ref. [41], which does not contradict the present observations because the total number of observed α decays in this study is low. From the four observed α-decay events, an α-particle energy of 8045(15) keV and a half-life of 35^{+32}_{-12} μs were extracted, latter with the exact maximum likelihood method of Ref. [42]. It is worth pointing out that this half-life is comparable but marginally shorter than that obtained earlier with better statistics from the internal-conversion events. Furthermore, an α-decay branch of 4(3)% was estimated from the number of observed α decays and internal-conversion events by taking into account the α-particle and simulated internal-conversion electron detection efficiencies, as well as the aforementioned tagging efficiency and calculated internal-conversion coefficient [39]. The quoted uncertainty is dominated by the statistical uncertainty arising from the low number of observed α-decay events.

IV. DISCUSSION

The presently measured $E_\alpha = 8045(15)$ keV for the ^{211m}Th corresponds to an energy release of 8200(15) keV in the α decay of the isomeric state. As the Q_α of ^{211}Th is 7943(14) keV [29] and the level energy of the final state of the α decay of ^{211m}Th is $E(^{207}\text{Ra}; (13/2^+)) = 554(15)$ keV [40], a level energy of 810(30) keV can be calculated for the ^{211m}Th. Furthermore, with the half-life and α-decay branch of 83(8) μs and 4(3)%, respectively, a reduced α-decay width of $\delta^2_\alpha = 170^{+200}_{-140}$ keV was extracted via the method of Rasmussen [43] by assuming s-wave α-particle emission. Once δ^2_α is normalized to the ground state-to-ground state α decay of the neighboring even-even isotopes ^{210,212}Th, an α-decay hindrance factor $H = 0.3^{+1.3}_{-0.2}$ can be obtained. As H is, within the present uncertainties, equal to unity, the initial- and final states of the ^{211m}Th α decay are likely to exhibit the same spin and parity. Based on the shell model and systematics arguments, the final state has been assigned tentatively to be $(13/2^+)$ [40], hence we propose the same spin and parity for the newly observed isomer in ^{211}Th. With similar arguments,

the ground state of ^{213}Th, ^{211}Th, and ^{207}Ra can be proposed to be $(5/2^-)$, $(3/2^-)$, and $(3/2^-)$, respectively.

The energy sum of the three internal transitions observed in this study is 778(8) keV, in good agreement with that obtained above from the α-decay data, further supporting the interpretation of the same origin. The internal branch depopulating the ^{211m}Th likely begins with the 203-keV $M2$ transition, feeding a $(9/2^-)$ state at 575 keV. As discussed above and as can be found in Ref. [27], a ground-state spin change from $(3/2^-)$ to $(5/2^-)$ takes place between ^{203,205}Rn, ^{207,209}Ra, and ^{211,213}Th along the isotopes of a given element. It is therefore reasonable to set a low-lying $(5/2^-)$ state in ^{211}Th, and place the 182-keV mixed character $M1/E2$ transition between that and the $(3/2^-)$ ground state. This leaves an opening in the level scheme for a transition of type $E2$, where we place the observed 393-keV transition.

The binding-energy surface[1] obtained via Hartree-Fock-Bogoliubov calculations [45] predict a shallow, weakly oblate (global) and prolate (local) minima for ^{211}Th. On the weakly oblate side a $\Omega = 3/2^-$ neutron orbital of the $f_{5/2}$ spherical parentage is likely to be occupied by the odd neutron of ^{211}Th, which explains the ground-state spin and parity proposed in this study. On the weakly prolate side of the Nilsson figure the $\Omega = 5/2^-$ and $\Omega = 13/2^+$ orbitals of $f_{5/2}$, and $i_{13/2}$ spherical origin, respectively, are close to the Fermi surface. Moving the odd neutron (hole) in this valence space provides a satisfactory explanation for the observed $(5/2^-)$ and $(13/2^+)$ states. Should this be the case, the presently observed isomeric state and the ground state of ^{211}Th would provide another example of coexisting different nuclear shapes (see, for example, Refs. [46–50] and references therein). The remaining $(9/2^-)$ state could be, for example, the $5/2^-$ state coupled to the collective 2^+ excitation of the underlying ^{210}Th core. Unfortunately $E(^{210}\text{Th}; 2^+)$ is not known, but with a robust extrapolation on the systematics [27] one may find a value comparable to the energy of the $E2$ transition observed in this study.

In Fig. 6 the present level energy is compared with those of other $13/2^+$ states observed in nearby even-Z odd-N nuclei. The newly obtained data appear to fit well to the systematic pattern set by these states, further supporting the $(13/2^+)$ assignment for the isomeric state in ^{211}Th. It is also apparent from Fig. 6 that the excitation energy of the isomer is not strongly dependent on proton number on a given isotone. This supports the suggested dominant neutron configuration of the wave function for the $13/2^+$ states. A $\nu i_{13/2}^{-1}$ configuration has been proposed for the isomer, for example, in $N = 121$ isotones ^{205}Po [51], ^{207}Rn [40], and ^{209}Ra [16], as well as for the $N = 123$ nuclei ^{207}Po [40], ^{209}Rn [52], ^{211}Ra [53], and ^{213}Th [19]. In said nuclei the $13/2^+$ state is depopulated via a hindered $M2$ transition. The inset of Fig. 6 displays the reduced transition strength of the $M2$ transition in these nuclei, with the newly obtained value of $B(M2) = 0.0025(5)$ W.u.

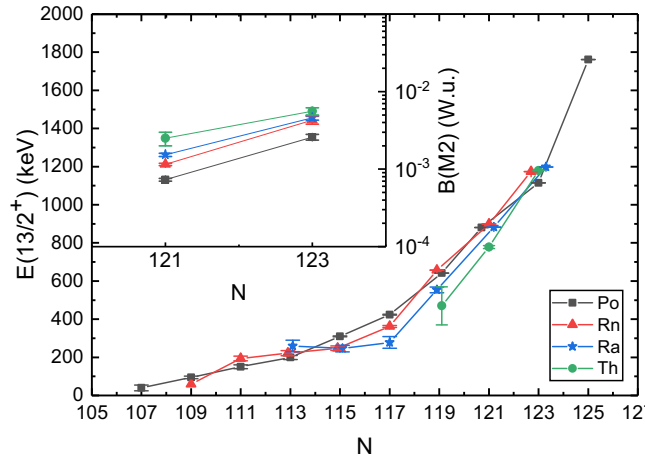

FIG. 6. Level energy systematics of the $13/2^+$ ($\nu i_{13/2}^{-1}$) isomeric state in Po, Rn, Ra, and Th nuclei. The inset provides the reduced transition strength of the $M2$ transition depopulating the state, if known. The data in this plot were obtained from this work and Refs. [13–15,17,19,33,40,51,52,54–60]. The neutron number of ^{211}Th is 121. Some of the I^π assignments in the literature are tentative.

being again in good agreement with those obtained from the literature, further supporting the proposed $\nu i_{13/2}^{-1}$ configuration for the $13/2^+$ state in ^{211}Th.

V. SUMMARY

An isomeric state with a half-life of 83(8) μs has been identified in ^{211}Th. This metastable state is dominantly depopulated via a hindered $M2$ transition with a strength of 0.0025(5) W.u., but also a weak α-decay branch of 4(3)% was observed. The α-decay hindrance factor implements favored decay, which in turn suggests a spin and parity of $13/2^+$ for the state. A $\nu i_{13/2}^{-1}$ configuration was proposed for the state based on the systematics. The present observations are in good agreement with the systematics of the same state in nearby nuclei.

ACKNOWLEDGMENTS

This work was supported by the Academy of Finland under the Contracts No. 213503 (Finnish Center of Excellence Programme) and No. 323710 (Personal research project, K.A.). The authors also thank the GAMMAPOOL European Spectroscopy Resource for the loan of the germanium detectors. The contribution of A.H. was supported by the Slovak Research and Development Agency (Contract No. APVV-15-0225), the Slovak grant agency VEGA (Contract No. 2/0129/17), and the project ITMS code 26210120023, supported by the Research and Development Operational Programme funded by ERDF (30%).

APPENDIX: PILE-UP CORRECTION

As evident from Fig. 4(d), more than half of the internal-conversion events of interest take place in the decay-time

[1]For the purposes of the following discussion we advise the reader to take a look at the binding-energy plot and the Nilsson diagram of ^{211}Th available in the AMEDEE database [44].

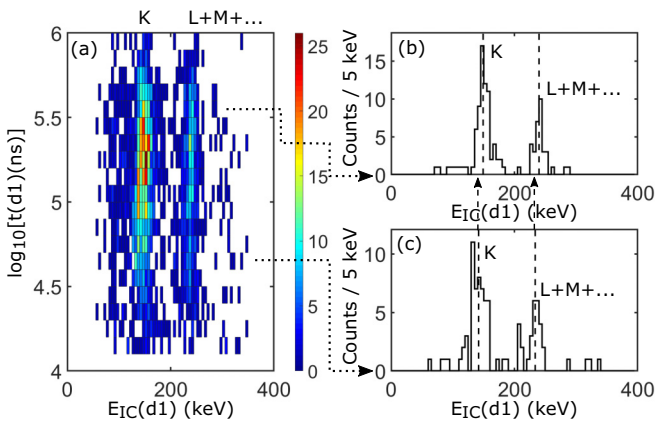

FIG. 7. (a) Decay time versus the measured energy of the internal-conversion electrons arising from the 238.4-keV $M2$ transition depopulating the known $^{13}/_{2}^{+}$ ($\nu i_{13/2}^{-1}$) isomeric state in ^{209}Ra [16]. Panels (b) and (c) are unshifted and shifted, respectively, example cuts of the data in panel (a) as indicated with the dotted lines. Dashed lines in panels (b) and (c) are the centroids of the K and $L + M + \cdots$ peaks extracted via a least-squares fit to the data. See text for further details.

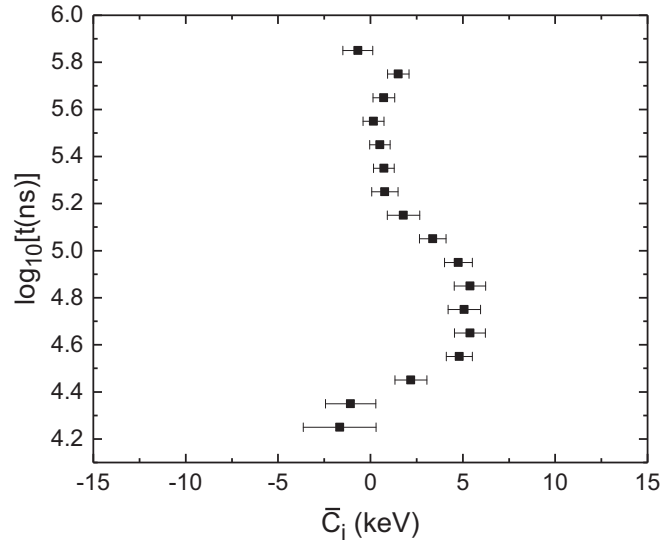

FIG. 8. Moving window correction $\bar{C}_i$ for a given time interval i to account for a shift in measured decay energy arising from the piling up of the implantation event and the subsequent fast decay event signals.

regime of $t(d1) \lesssim 100$ μs. The signal of these events is likely to pile up with that of the preceding recoil implantation in a way that might impact the registered electron energy. Therefore, additional correction is needed. This correction was obtained via the conversion electrons associated with the 238.4-keV $M2$ transition depopulating the known $^{13}/_{2}^{+}$ ($\nu i_{13/2}^{-1}$) isomeric state in ^{209}Ra [16], which are available in large quantities in our data. These events were selected in similar manner as those in Fig. 4(c), but with the time conditions of $t(d1) < 1$ ms and $t(d2) < 16$ s and by setting a gate on $E(d2)$ that reflects the α-particle energy of ^{209}Ra. Obtained data were then sorted in a matrix containing the measured energy and decay time as displayed in Fig. 7(a). Each row of the matrix contains the energy spectrum of the events that appeared on a certain time interval. Two examples are provided in Figs. 7(b) and 7(c), as indicated with the dotted arrows. The centroid of each K and $L + M + \cdots$ peak on each time interval was then obtained by fitting a Gaussian shape into the peaks. The dashed lines in Figs. 7(b) and 7(c) demonstrate an apparent shift between the centroids of the "slow" and "fast" events. The long-living (unshifted) time intervals were then used to form a reference value. The average shift C_i between the reference and the measured energy was calculated as $C_i = {}^{1}/_{2}[\Delta E_i(K) + \Delta E_i(L + M + \cdots)]$ for each time interval i. Finally, a correction $\bar{C}_i$ for a given time interval was obtained as a moving window average

$$\bar{C}_i = {}^{1}/_{4}[C_{i-1} + 2C_i + C_{i+1}], \tag{A1}$$

which is displayed in Fig. 8, and it was applied on event-by-event basis in order to obtain the spectrum displayed in Fig. 4(c).

[1] G. D. Dracoulis, P. M. Walker, and F. G. Kondev, Rep. Prog. Phys. **79**, 076301 (2016).

[2] P. Walker and G. Dracoulis, Nature (London) **399**, 35 (1999).

[3] P. Walker and J. Carroll, Phys. Today **58**, 39 (2005).

[4] M. Arnould, S. Goriely, and K. Takahashi, Phys. Rep. **450**, 97 (2007).

[5] A. B. Hayes, D. Cline, K. J. Moody, I. Ragnarsson, C. Y. Wu, J. A. Becker, M. P. Carpenter, J. J. Carroll, D. Gohlke, J. P. Greene, A. A. Hecht, R. V. F. Janssens, S. A. Karamian, T. Lauritsen, C. J. Lister, R. A. Macri, R. Propri, D. Seweryniak, X. Wang, R. Wheeler *et al.*, Phys. Rev. C **82**, 044319 (2010).

[6] I. Stefanescu, G. Georgiev, F. Ames, J. Aysto, D. L. Balabanski, G. Bollen, P. A. Butler, J. Cederkall, N. Champault, T. Davinson, A. DeMaesschalck, P. Delahaye, J. Eberth, D. Fedorov, V. N. Fedosseev, L. M. Fraile, S. Franchoo, K. Gladnishki, D. Habs, K. Heyde *et al.*, Phys. Rev. Lett. **98**, 122701 (2007).

[7] D. Santiago-Gonzalez, K. Auranen, M. L. Avila, A. D. Ayangeakaa, B. B. Back, S. Bottoni, M. P. Carpenter, J. Chen, C. M. Deibel, A. A. Hood, C. R. Hoffman, R. V. F. Janssens, C. L. Jiang, B. P. Kay, S. A. Kuvin, A. Lauer, J. P. Schiffer, J. Sethi, R. Talwar, I. Wiedenhöver *et al.*, Phys. Rev. Lett. **120**, 122503 (2018).

[8] M. C. Lewis, E. Parr, R. D. Page, C. McPeake, D. T. Joss, F. A. Ali, K. Auranen, A. D. Briscoe, L. Capponi, T. Grahn, P. T. Greenlees, J. Henderson, A. Herzan, U. Jakobsson, R. Julin, S. Juutinen, J. Konki, M. Labiche, M. Leino, P. J. R. Mason, M. Nyman, D. O'Donnell, J. Pakarinen *et al.*, Phys. Rev. C **98**, 024302 (2018).

[9] J. Kallunkathariyil, B. Sulignano, P. T. Greenlees, J. Khuyagbaatar, C. Theisen, K. Auranen, H. Badran, F. Bisso,

P. Brionnet, R. Briselet, A. Drouart, Z. Favier, T. Goigoux, T. Grahn, K. Hauschild, A. Herzan, F. P. Hessberger, U. Jakobsson, R. Julin, S. Juutinen, J. Konki *et al.*, Phys. Rev. C **101**, 011301(R) (2020).

[10] M. G. Procter, D. M. Cullen, M. J. Taylor, J. Pakarinen, K. Auranen, T. Bäck, T. Braunroth, B. Cederwall, A. Dewald, T. Grahn, P. T. Greenlees, U. Jakobsson, R. Julin, S. Juutinen, A. Herzáň, J. Konki, M. Leino, R. Liotta, J. Partanen, P. Peura *et al.*, Phys. Rev. C **87**, 014308 (2013).

[11] K. Auranen, J. Uusitalo, S. Juutinen, U. Jakobsson, T. Grahn, P. T. Greenlees, K. Hauschild, A. Herzáň, R. Julin, J. Konki, M. Leino, J. Pakarinen, J. Partanen, P. Peura, P. Rahkila, P. Ruotsalainen, M. Sandzelius, J. Sarén, C. Scholey, J. Sorri *et al.*, Phys. Rev. C **90**, 024310 (2014).

[12] K. Auranen, J. Uusitalo, S. Juutinen, H. Badran, F. D. Bisso, D. Cox, T. Grahn, P. T. Greenlees, A. Herzáň, U. Jakobsson, R. Julin, J. Konki, M. Leino, A. Lightfoot, M. Mallaburn, O. Neuvonen, J. Pakarinen, P. Papadakis, J. Partanen, P. Rahkila *et al.*, Phys. Rev. C **95**, 044311 (2017).

[13] N. A. Althubiti, D. Atanasov, K. Blaum, T. E. Cocolios, T. Day Goodacre, G. J. Farooq-Smith, D. V. Fedorov, V. N. Fedosseev, S. George, F. Herfurth, K. Heyde, S. Kreim, D. Lunney, K. M. Lynch, V. Manea, B. A. Marsh, D. Neidherr, M. Rosenbusch, R. E. Rossel, S. Rothe *et al.* (ISOLTRAP Collaboration), Phys. Rev. C **96**, 044325 (2017).

[14] R. E. Stone, C. R. Bingham, L. L. Riedinger, R. W. Lide, H. K. Carter, R. L. Mlekodaj, and E. H. Spejewski, Phys. Rev. C **31**, 582 (1985).

[15] A. Y. Deo, Z. Podolyák, P. M. Walker, A. Algora, B. Rubio, J. Agramunt, L. M. Fraile, N. Al-Dahan, N. Alkhomashi, J. A. Briz, E. Estevez, G. Farrelly, W. Gelletly, A. Herlert, U. Köster, A. Maira, and S. Singla, Phys. Rev. C **81**, 024322 (2010).

[16] K. Hauschild, A. Lopez-Martens, A. V. Yeremin, O. Dorvaux, A. V. Belozerov, M. L. Chelnokov, V. I. Chepigin, B. Gall, V. A. Gorshkov, M. Guttormsen, P. Jones, A. P. Kabachenko, A. Khouaja, A. C. Larsen, O. N. Malyshev, A. Minkova, H. T. Nyhus, Y. T. Oganessian, D. Pantelica, A. G. Popeko *et al.*, Phys. Rev. C **77**, 047305 (2008).

[17] Z. Kalaninová, S. Antalic, A. N. Andreyev, F. P. Heßberger, D. Ackermann, B. Andel, L. Bianco, S. Hofmann, M. Huyse, B. Kindler, B. Lommel, R. Mann, R. D. Page, P. J. Sapple, J. Thomson, P. Van Duppen, and M. Venhart, Phys. Rev. C **89**, 054312 (2014).

[18] J. A. Heredia, A. N. Andreyev, S. Antalic, S. Hofmann, D. Ackermann, V. F. Comas, S. Heinz, F. P. Heßberger, B. Kindler, J. Khuyagbaatar, B. Lommel, and R. Mann, Eur. Phys. J. A **46**, 337 (2010).

[19] J. Khuyagbaatar, S. Hofmann, F. P. Heßberger, D. Ackermann, S. Antalic, H. G. Burkhard, S. Heinz, B. Kindler, A. F. Lisetskiy, B. Lommel, R. Mann, K. Nishio, H. J. Schött, and B. Sulignano, Eur. Phys. J. A **34**, 355 (2007).

[20] B. Jonson, M. Alpsten, Å. Appelqvist, and G. Astner, Nucl. Phys. A **174**, 225 (1971).

[21] M. Leino, J. Äystö, T. Enqvist, P. Heikkinen, A. Jokinen, M. Nurmia, A. Ostrowski, W. Trzaska, J. Uusitalo, K. Eskola, P. Armbruster, and V. Ninov, Nucl. Instrum. Methods Phys. Res., Sect. B **99**, 653 (1995).

[22] J. Sarén, J. Uusitalo, M. Leino, and J. Sorri, Nucl. Instrum. Methods Phys. Res., Sect. A **654**, 508 (2011).

[23] R. Page, A. Andreyev, D. Appelbe, P. Butler, S. Freeman, P. Greenlees, R.-D. Herzberg, D. Jenkins, G. Jones, P. Jones, D. Joss, R. Julin, H. Kettunen, M. Leino, P. Rahkila, P. Regan, J. Simpson, J. Uusitalo, S. Vincent, and R. Wadsworth, Nucl. Instrum. Methods Phys. Res., Sect. B **204**, 634 (2003).

[24] K. Auranen, U. Jakobsson, H. Badran, T. Grahn, P. T. Greenlees, A. Herzáň, R. Julin, S. Juutinen, J. Konki, M. Leino, A.-P. Leppänen, G. O'Neill, J. Pakarinen, P. Papadakis, J. Partanen, P. Rahkila, P. Ruotsalainen, M. Sandzelius, J. Sarén, C. Scholey *et al.*, Phys. Rev. C **101**, 024306 (2020).

[25] G. Duchêne, F. Beck, P. Twin, G. de France, D. Curien, L. Han, C. Beausang, M. Bentley, P. Nolan, and J. Simpson, Nucl. Instrum. Methods Phys. Res., Sect. A **432**, 90 (1999).

[26] P. Rahkila, Nucl. Instrum. Methods Phys. Res., Sect. A **595**, 637 (2008).

[27] Nudat2.6, http://www.nndc.bnl.gov/nudat2/.

[28] K. Auranen, J. Uusitalo, H. Badran, T. Grahn, P. T. Greenlees, A. Herzáň, U. Jakobsson, R. Julin, S. Juutinen, J. Konki, M. Leino, A.-P. Leppänen, G. O'Neill, J. Pakarinen, P. Papadakis, J. Partanen, P. Peura, P. Rahkila, P. Ruotsalainen, M. Sandzelius *et al.*, Phys. Rev. C **102**, 034305 (2020).

[29] J. Uusitalo, T. Enqvist, M. Leino, W. H. Trzaska, K. Eskola, P. Armbruster, and V. Ninov, Phys. Rev. C **52**, 113 (1995).

[30] D. Vermeulen, H.-G. Clerc, W. Lang, K. H. Schmidt, and G. Münzenberg, Z. Phys. A: At. Nucl. A (1975) **294**, 149 (1980).

[31] F. Kondev, Nucl. Data Sheets **109**, 1527 (2008).

[32] F. P. Hessberger, S. Hofmann, and D. Ackermann, Eur. Phys. J. A **16**, 365 (2003).

[33] F. Kondev, Nucl. Data Sheets **105**, 1 (2005).

[34] A. Rytz, At. Data Nucl. Data Tables **47**, 205 (1991).

[35] R. B. E. Taylor, S. J. Freeman, J. L. Durell, M. J. Leddy, A. G. Smith, D. J. Blumenthal, M. P. Carpenter, C. N. Davids, C. J. Lister, R. V. F. Janssens, and D. Seweryniak, Phys. Rev. C **54**, 2926 (1996).

[36] K. Schmidt, Eur. Phys. J. A **8**, 141 (2000).

[37] C. Theisen, A. Lopez-Martens, and C. Bonnelle, Nucl. Instrum. Methods Phys. Res., Sect. A **589**, 230 (2008).

[38] F. Hessberger, S. Hofmann, G. Münzenberg, K.-H. Schmidt, P. Armbruster, and R. Hingmann, Nucl. Instrum. Methods Phys. Res., Sect. A **274**, 522 (1989).

[39] T. Kibédi, T. Burrows, M. Trzhaskovskaya, P. Davidson, and C. N. Jr., Nucl. Instrum. Methods Phys. Res., Sect. A **589**, 202 (2008).

[40] F. Kondev and S. Lalkovski, Nucl. Data Sheets **112**, 707 (2011).

[41] F. P. Heßberger, S. Hofmann, G. Münzenberg, A. B. Quint, K. Sümmerer, and P. Armbruster, Europhys. Lett. **3**, 895 (1987).

[42] K. H. Schmidt, C. C. Sahm, K. Pielenz, and H. G. Clerc, Z. Phys. A: At. Nucl. (1975) **316**, 19 (1984).

[43] J. O. Rasmussen, Phys. Rev. **113**, 1593 (1959).

[44] S. Hilaire and M.Girod, http://www-phynu.cea.fr/science_en_ligne/carte_potentiels_microscopiques/carte_potentiel_nucleaire_eng.htm AMEDEE database, accessed May 28, 2020.

[45] S. Hilaire and M. Girod, Eur. Phys. J. A **33**, 237 (2007).

[46] K. Heyde, P. V. Isacker, M. Waroquier, J. Wood, and R. Meyer, Phys. Rep. **102**, 291 (1983).

[47] J. Wood, K. Heyde, W. Nazarewicz, M. Huyse, and P. van Duppen, Phys. Rep. **215**, 101 (1992).

[48] R. Julin, K. Helariutta, and M. Muikku, J. Phys. G **27**, R109 (2001).
[49] K. Heyde and J. L. Wood, Rev. Mod. Phys. **83**, 1467 (2011).
[50] R. Julin, T. Grahn, J. Pakarinen, and P. Rahkila, J. Phys. G **43**, 024004 (2016).
[51] F. Kondev, Nucl. Data Sheets **101**, 521 (2004).
[52] J. Chen and F. Kondev, Nucl. Data Sheets **126**, 373 (2015).
[53] F. P. Heßberger, S. Hofmann, I. Kojouharov, and D. Ackermann, Eur. Phys. J. A **22**, 253 (2004).
[54] A. N. Andreyev, M. Huyse, K. Van de Vel, P. Van Duppen, O. Dorvaux, P. Greenlees, K. Helariutta, P. Jones, R. Julin, S. Juutinen, H. Kettunen, P. Kuusiniemi, M. Leino, M. Muikku, P. Nieminen, P. Rahkila, J. Uusitalo, R. Wyss, K. Hauschild, and Y. Le Coz, Phys. Rev. C **66**, 014313 (2002).
[55] J. Sauvage, B. Roussière, J. Genevey, S. Franchoo, A. N. Andreyev, N. Barré, A. Ben Braham, C. Bourgeois, J.-F. Clavelin, H. De Witte, D. V. Fedorov, V. N. Fedoseyev, L. M. Fraile, X. Grave, G. Huber, M. Huyse, P. Kilcher, U. Köster, P. Kunz, S. R. Lesher *et al.*, Eur. Phys. J. A **49**, 109 (2013).
[56] F. Kondev, Nucl. Data Sheets **108**, 365 (2007).
[57] J. Uusitalo, H. Kettunen, A. Andreyev, K. Eskola, P. Greenlees, K. Helariutta, M. Huyse, P. Jones, R. Julin, S. Juutinen, H. Kankaanpää, P. Kuusiniemi, M. Leino, M. Muikku, P. Nieminen, P. Rahkila, K. Van de Vel, and P. Van Duppen, Acta Phys. Pol. B **32**, 1015 (2001).
[58] B. Singh, D. Abriola, C. Baglin, V. Demetriou, T. Johnson, E. McCutchan, G. Mukherjee, S. Singh, A. Sonzogni, and J. Tuli, Nucl. Data Sheets **114**, 661 (2013).
[59] G. Audi, F. G. Kondev, M. Wang, W. Huang, and S. Naimi, Chin. Phys. C **41**, 030001 (2017).
[60] H. B. Zhou, Z. G. Gan, N. Wang, H. B. Yang, L. Ma, M. H. Huang, C. L. Yang, M. M. Zhang, Y. L. Tian, Y. S. Wang, Z. Y. Li, C. X. Yuan, S. Huang, X. J. Sun, H. Y. Peng, L. Ou, and X. H. Zhou, Phys. Rev. C **103**, 044314 (2021).